ARTICLES
PUBLISHED ONLINE: 9 MARCH 2015 | DOI: 10.1038/NMAT4228
nature materials

In situ atomic-scale observation of twinning-dominated deformation in nanoscale body-centred cubic tungsten

Jiangwei Wang[1], Zhi Zeng[2], Christopher R. Weinberger[3,4]*, Ze Zhang[5], Ting Zhu[2,6]* and Scott X. Mao[1,5]*

Twinning is a fundamental deformation mode that competes against dislocation slip in crystalline solids. In metallic nanostructures, plastic deformation requires higher stresses than those needed in their bulk counterparts, resulting in the 'smaller is stronger' phenomenon. Such high stresses are thought to favour twinning over dislocation slip. Deformation twinning has been well documented in face-centred cubic (FCC) nanoscale crystals. However, it remains unexplored in body-centred cubic (BCC) nanoscale crystals. Here, by using *in situ* high-resolution transmission electron microscopy and atomistic simulations, we show that twinning is the dominant deformation mechanism in nanoscale crystals of BCC tungsten. Such deformation twinning is pseudoelastic, manifested through reversible detwinning during unloading. We find that the competition between twinning and dislocation slip can be mediated by loading orientation, which is attributed to the competing nucleation mechanism of defects in nanoscale BCC crystals. Our work provides direct observations of deformation twinning as well as new insights into the deformation mechanism in BCC nanostructures.

The past decade has witnessed a marked increase in the study of mechanical properties and deformation mechanisms in metallic nanostructures[1–5]. In this field, one prominent approach is to conduct *in situ* mechanical testing of nanostructures[5–12]. These real-time experiments have revealed a wealth of novel deformation behaviours and size effects in various kinds of nanoscale crystals, including dislocation starvation[13], mechanical annealing[6], surface-dislocation-controlled yielding[8,9], twinning-dominated deformation[14–16] and surface-diffusion-mediated pseudoelasticity[17]. However, the majority of those results are obtained for FCC nanostructures. Given the widespread use of bulk BCC metals, BCC nanostructures are expected to play significant roles in future nanotechnologies[18–20]. Hence it is natural to ask to what degree these phenomena and size effects in nanoscale FCC crystals still hold in nanoscale BCC crystals.

One fundamental question regarding the deformation mechanism of metallic nanostructures is whether or not the material will deform via twinning[21–23]. Deformation twinning is commonly observed in hexagonal-close packed (HCP) crystals[3,7,24,25], but is much less common in bulk FCC and BCC crystals. Deformation twinning in these materials usually occurs under high strain rates or low temperatures[25–27], conditions that lead to high stresses. High stresses are readily achieved in nanoscale crystals[1,5], resulting from the starvation of plastic deformation carriers in these small crystals due to their large surface area to volume ratio. Such high stresses are thought to favour twinning even at room temperature and low strain rates, which can critically affect mechanical properties such as strength and ductility of metallic nanostructures[3,11,16]. Recently, both *in situ* and *ex situ* nanomechanical experiments have revealed deformation twinning in FCC nanostructures, including Au nanowhiskers[14] and Cu nanowires[15]. In contrast, the mechanical testing of small-volume BCC crystals has reported only dislocation-mediated plasticity, for example, in single-crystalline W, Mo, Ta, Nb, V and Fe nanowires or nanopillars[10,12,28–31] and Mo alloy nanofibres[32]. In mechanical testing experiments where TEM analysis was not used, and thus dislocations were not observed, the deformation is still attributed to dislocation plasticity[33,34]. Deformation twinning was reported in nanocrystalline Ta (ref. 35); however a close examination of this experiment shows that the observed twinning probably occurred in small grains of FCC Ta, instead of BCC Ta (see Supplementary Discussion 1).

In bulk BCC metals, deformation at room temperature is usually controlled by dislocations with high lattice resistances[12,31,36–40]. In small-scale BCC crystals, the large surface area tends to destabilize bulk dislocation sources. As a result, nucleation of defects from the surface, including dislocations and twins, becomes a competing deformation mode at room temperature and low strain rates; twinning could dominate when its nucleation from the surface is easier than that of a dislocation.

To understand the controlling deformation mechanisms in small-scale BCC metals, here we investigate nanoscale BCC tungsten (W) crystals using *in situ* nanomechanical testing with high-resolution TEM (HRTEM). To achieve this, we develop an *in situ* welding process to fabricate the W nanowires (Methods). This method overcomes the difficulties of synthesizing sub-100 nm BCC samples without pre-existing defects, in contrast to the commonly

[1]Department of Mechanical Engineering and Materials Science, University of Pittsburgh, Pittsburgh, Pennsylvania 15261, USA. [2]Woodruff School of Mechanical Engineering, Georgia Institute of Technology, Atlanta, Georgia 30332, USA. [3]Materials Science and Engineering Center, Sandia National Laboratories, Albuquerque, New Mexico 87185, USA. [4]Department of Mechanical Engineering and Mechanics, Drexel University, Philadelphia, Pennsylvania 19104, USA. [5]Department of Materials Science and Engineering and State Key Laboratory of Silicon Materials, Zhejiang University, Hangzhou 310027, China. [6]School of Materials Science and Engineering, Georgia Institute of Technology, Atlanta, Georgia 30332, USA.
*e-mail: cweinberger@coe.drexel.edu; ting.zhu@me.gatech.edu; sxm2@pitt.edu

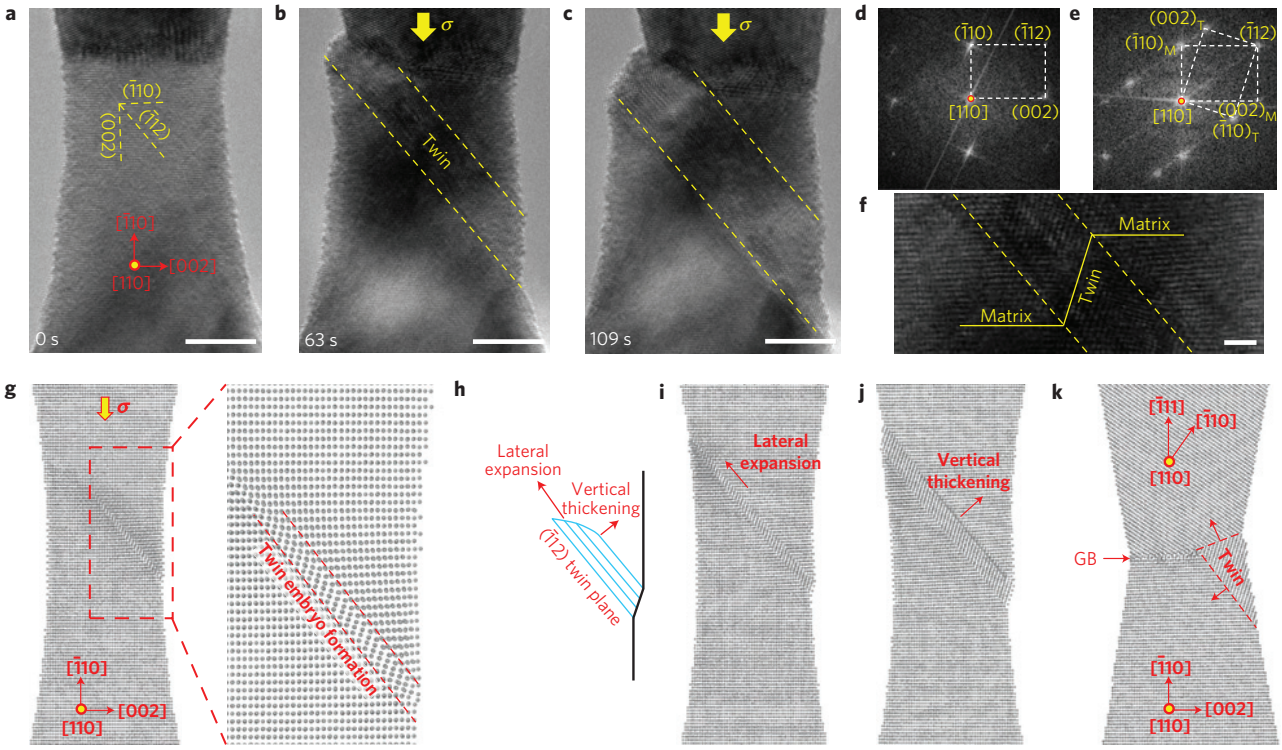

Figure 1 | Deformation twinning in a W bicrystal nanowire under [1̄10] compression. a–c, Sequential TEM images showing deformation twinning in a W bicrystal nanowire (15 nm in diameter) at room temperature under a strain rate of 10^{-3} s^{-1}, which is loaded along [1̄10] and viewed along [110]. Scale bars, 5 nm. **d**,**e**, Fast Fourier transform pattern of the pristine W bicrystal and the deformation twin, respectively. **f**, Magnified TEM image showing the deformation twin. Scale bar, 1 nm. **g**, MD snapshot and zoomed-in image showing the nucleation of a deformation twin embryo in a W single-crystal nanowire. **h**, Schematic of the lateral expansion and vertical thickening of a twin band. **i**,**j**, MD snapshots showing the lateral expansion and vertical thickening of a deformation twin. **k**, Nucleation and thickening of a deformation twin in a W bicrystal nanowire. The crystal orientation is the same as that in Supplementary Fig. 2.

used sample preparation by the focused ion beam method, which tends to create feature sizes larger than 100 nm as well as surface damage[6,7,12,13]. Using these *in situ* fabricated samples, we demonstrate that twinning is the dominant deformation mechanism in nanoscale W crystals at room temperature and low strain rates. Such mechanical twinning is pseudoelastic, as evidenced by the reversible detwinning during unloading. We further find that the loading orientation governs the competition between twinning and dislocation slip. Atomistic simulations are performed to provide insights into the twinning-dominated deformation mechanism in those nanoscale BCC crystals.

Figure 1 and Supplementary Movie 1 show the *in situ* uniaxial compression of a W bicrystal nanowire at room temperature under a strain rate of $\sim 10^{-3}$ s^{-1}. This sample contains a large single crystal whose [1̄10] direction is aligned with the overall axial direction of the bicrystal nanowire. Since the deformation events are primarily observed in this large crystal, the bicrystal sample is referred to as a [1̄10]-oriented nanowire. TEM imaging is aligned with the transverse [110] direction (Fig. 1a). On compressive loading, the nanowire initially undergoes elastic deformation. As the lattice strain in the relatively large [1̄10]-oriented crystal accumulates to around 4.9% (Supplementary Fig. 1), a small twin embryo nucleates from the intersection between the grain boundary and free surface, and transverses the entire sample under continued loading (Fig. 1b). Figure 1d–f confirms that the observed deformation band in the [1̄10]-oriented crystal is a twin band with the active twinning system of [1$\bar{1}$1](1̄12), as evidenced by the Fast Fourier transform pattern (Fig. 1d–e) and zoomed-in image (Fig. 1f). At the onset of twinning, the resolved shear stress on the (1̄12) plane on which the twin forms is estimated to be about 9 GPa, based on the lattice strain (Supplementary Fig. 1). After a complete twin band forms, the lattice strain is released to about 1.3% (Supplementary Fig. 1). A further increase in the applied load causes thickening of the twin band, thus producing an increased amount of inelastic strain (Fig. 1c). Moreover, we observe that the grain boundary alone can serve as the effective nucleation site for deformation twins (Twin 2 in Supplementary Fig. 2 and Supplementary Movie 2).

To understand the twinning mechanism in nanoscale W crystals, we performed molecular dynamics (MD) simulations of both single-crystal and bicrystal W nanowires (Fig. 1g–k). In the [1̄10]-oriented single crystal, a twin embryo initially forms from the surface (Fig. 1g) and expands laterally to penetrate the whole nanowire (Fig. 1h,i). Then the twin band thickens through layer-by-layer vertical growth at the twin boundary via sequential nucleation of 1/6[1$\bar{1}$1] twinning dislocations on adjacent (1̄12) planes (Fig. 1j). The resolved shear stress on the (1̄12) plane for twin formation in MD is about 8 GPa, which is of the same order as the experimental estimate. The bicrystal nanowire in MD exhibits twin nucleation and thickening from the intersection between grain boundary and free surface (Fig. 1k), which penetrates into both crystals, similar to the observations in some of our experiments (Twin 1 in Supplementary Fig. 2). These atomistic studies also show that deformation twinning in nanoscale W crystals is controlled by surface nucleation. Irrespective of types of surface sites and shear modes used in simulations, the twin embryo is always able to nucleate from the free surface and expand into a twin band in a [1̄10]-oriented W nanowire at the characteristic load level measured in experiments (Supplementary Discussion 2). Overall, these MD results compare favourably with our experimental observations.

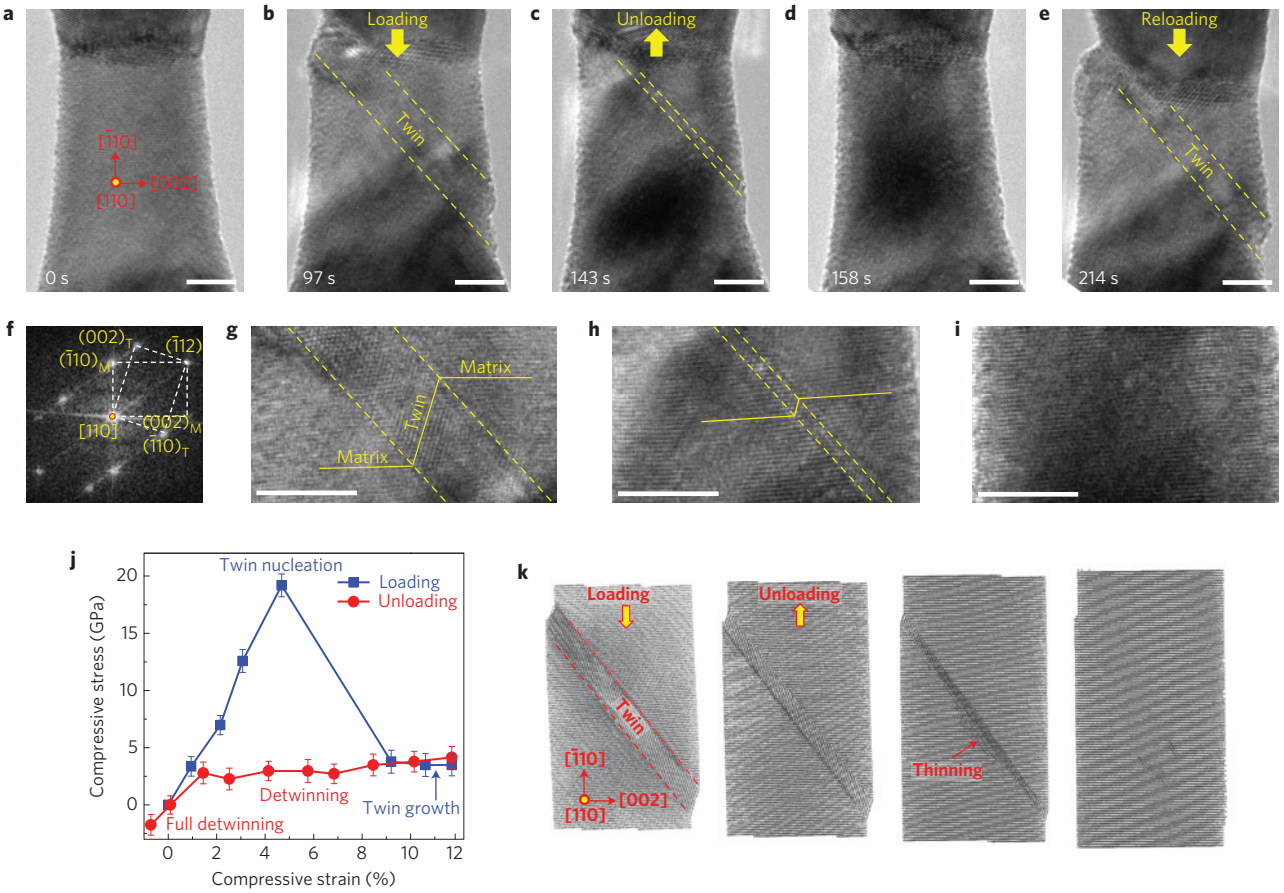

Figure 2 | Reversible deformation twinning and detwinning processes in a W bicrystal nanowire under cyclic loading. a, Pristine W bicrystal nanowire with a diameter 14.7 nm as viewed along [110] and loaded along [1̄10]. **b**,**g**, Under compression, the deformation twin nucleates and expands to about 4 nm in thickness. **c**,**h**, A layer-by-layer detwinning process occurs on unloading (also see Supplementary Movie 3). **d**,**i**, After complete detwinning, the W bicrystal recovers its original shape. **e**, A deformation twin nucleates at the same place in subsequent deformation cycles. **f**, Fast Fourier transform pattern of the deformation twin. **j**, Stress versus strain curve during compressive loading and unloading, showing the pseudoelastic response. The stress is estimated on the basis of the lattice strain and the overall compressive strain is measured from the change of the nanowire length. The error bars represent the variations of the estimated stresses at different locations of the nanowire. **k**, MD snapshots showing the twinning–detwinning process similar to TEM observations. All scale bars, 5 nm.

Deformation twinning in W bicrystals is pseudoelastic, as manifested in experiments through reversible detwinning on unloading. That is, during compressive loading, the W bicrystal experiences large deformation via the formation of a deformation twin (Fig. 2a,b,f,g), the thickness of which is about 4 nm just before unloading (Fig. 2g). However, on unloading, deformation mainly occurs at the twin boundary via a process of layer-by-layer detwinning (Fig. 2c,h and Supplementary Movie 3). Namely, detwinning proceeds in the same fashion as twinning through the nucleation and propagation of twinning dislocations, but in the reverse direction. As a result, the twin thickness is gradually reduced, returning the bicrystal to its original shape without apparent defects after a complete unloading (Fig. 2d,i). Pseudoelasticity is also manifested in the stress–strain curve, which demonstrates the recovery of the initial zero stress and strain values after a loading/unloading cycle (Fig. 2j). During multiple loading/unloading cycles, the deformation twin is always observed to nucleate at the same location (Fig. 2e). Such pseudoelastic twinning is also observed in our MD simulations. Figure 2k shows MD snapshots of a detwinning process during unloading, which occurs layer-by-layer at the twin boundary via $1/6[\bar{1}1\bar{1}]$ detwinning dislocations nucleated on adjacent $(\bar{1}12)$ planes, consistent with TEM observations. Detwinning in experiments can be attributed to the interplay between the unloading and the deformation incompatibility at the intersection between grain boundary and twin band. Specifically, a twin forms under the applied compressive load and thickens as the nanowire is further compressed. In other words, a twin thickens because the driving force of axial compression (giving the resolved shear stress on the twinning system) is able to overcome the twinning resistance, such as the back stress arising from the deformation incompatibility at the intersection between twin band and grain boundary. When the applied compression is reduced during unloading, detwinning occurs since the resolved shear stress for twinning becomes less than the back stress for detwinning. Such back stress can cause the formation of $1/6[\bar{1}1\bar{1}]$ detwinning dislocations near the grain boundary, whose glide along the $(\bar{1}12)$ twin boundary leads to the thinning of the twin band. This grain-boundary-mediated detwinning process has been observed in our MD simulations (Supplementary Fig. 3).

In addition to the ⟨110⟩ loading, we observe that deformation twinning dominates for several other loading orientations tested, including ⟨100⟩ tension and ⟨111⟩ compression (Supplementary Fig. 4). However, we find that dislocation slip prevails under ⟨112⟩ loading, for both tension and compression (Fig. 3 and Supplementary Figs 5–7). Figure 3 and Supplementary Movie 4 show the dislocation-mediated plastic deformation of a W bicrystal under [112] compression. Initially, the bicrystal is nearly pristine, without observable dislocations (Supplementary Fig. 5a). Under

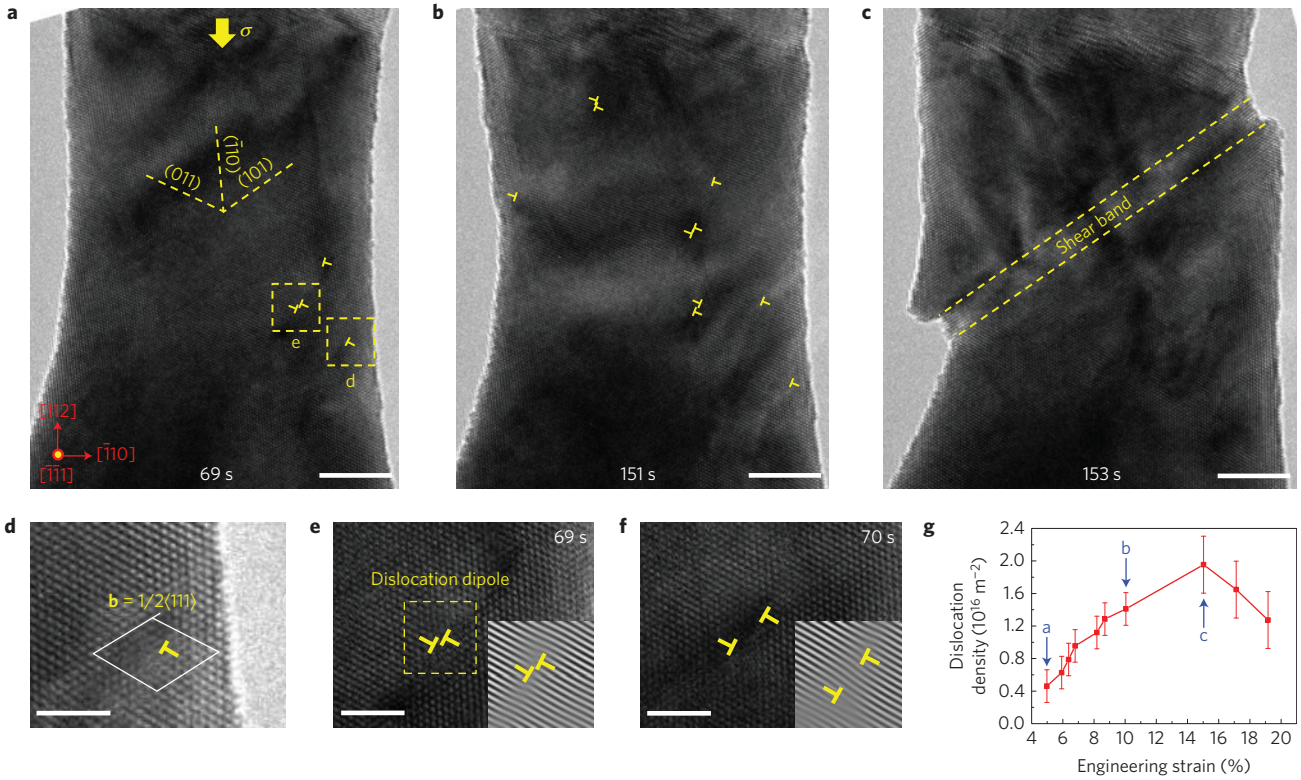

Figure 3 | Dislocation dynamics inside a W bicrystal nanowire under [112] compression. a–c, Sequential TEM images showing the deformation of a W bicrystal nanowire (21 nm in diameter) under [112] compression, as viewed along [$\bar{1}\bar{1}$1], exhibiting the nucleation of dislocations and the formation of a shear band. Dislocations are marked by an upside-down 'T'. **d**, Analysis of the Burgers vector, **b**, of a dislocation nucleated from the side surface indicates a 1/2⟨111⟩-type mixed dislocation. **e**,**f**, Sequential TEM images showing the nucleation and expansion of a dislocation dipole under [112] compression. **g**, The dislocation density versus the compressive strain; blue arrows indicate the states of deformation shown in the TEM images of **a–c**. The error bars represent the variations of dislocation density from repeated measurements. Scale bars in **a–c**, 5 nm; **d–f**, 2 nm.

compressive loading, dislocations nucleate simultaneously from multiple sources, with the estimated shear stress of about 7.2 GPa on the (101) slip plane (Fig. 3a,b), leading to the yielding of this W bicrystal. Most dislocations seem to nucleate as dipoles (Fig. 3b), which are probably half dislocation loops on (101) planes. These dislocation dipoles are mobile, resulting in their expansion on the (101) slip planes after nucleation (Fig. 3e,f). Further deformation causes the formation and thickening of a shear band on the (101) plane, within which the dislocation density is as high as $\sim 2 \times 10^{16}$ m^{-2}, thus generating a large local plastic strain (Fig. 3c,g and Supplementary Figs 5–6). Incidentally, it has been notoriously difficult to determine the operative dislocation slip planes in BCC metals[41,42], and the commonly used visual inspection of slip traces often caused confusion as to the {110} versus {112} slip[41]. In contrast, our *in situ* HRTEM experiments enable a direct unambiguous determination of the active slip plane in BCC crystals—that is, a specific {110} plane whose activation is presumably due to the large resolved shear stress. While the recent work by Caillard reported TEM observations of {110} slip in iron[43], our method provides a way to directly view the active slip planes and is a complementary technique to that used by Caillard for the determination of slip planes in BCC metals.

To understand the competition between deformation twinning and dislocation slip, we perform atomistic studies of W single crystals under ⟨112⟩ loading. In our direct MD simulations, either tension or compression, deformation is dominated by dislocation slip, including the nucleation of dislocations from the surface, their subsequent glide inside the crystal and entanglement with each other; some dislocations eventually escape from other parts of the surface under continued loading (Supplementary Fig. 8). While MD simulations are consistent with experimental observations, one might still question why dislocation slip is the active deformation mode under ⟨112⟩ loading, while twinning dominates under other loading orientations tested, including ⟨110⟩, ⟨100⟩ and ⟨111⟩.

To further investigate the competition between twinning and dislocation slip, we note that a surface-emanated defect in small BCC crystals can experience large resistances concurrently from both the surface and lattice. As a result, even if a surface defect such as a twin embryo has been emanated at some favourable surface site, its expansion in the nucleation process, as schematically shown in Fig. 1h, still has to compete with other modes of defect nucleation. To explore such competition of nucleation, we create a twin embryo near the surface of a [112]-oriented W crystal (Fig. 4a). This embryo belongs to the [$\bar{1}\bar{1}$1](211) twin system, which is subjected to the largest resolved shear stress among all possible twinning systems under [112] compression. During molecular statics relaxations under various applied stresses, we always observe the nucleation of individual dislocation loops from the edge of the twin embryo rather than the expansion of the twin embryo itself. Similar dislocation-dominated responses are observed when a twin embryo is created at other surface locations (for example, Fig. 4b). These results demonstrate that the nucleation of the twin embryo can be limited by lateral expansion during its nucleation process under [112] compression. In contrast, for other loading orientations studied, the twin embryo created at the surface always forms a complete twin band and then thickens through layer-by-layer migration of the twin boundary, as seen during [110] compression (Supplementary Discussion 2). These atomistic studies clearly demonstrate the surface-nucleation-controlled deformation mechanisms in nanoscale BCC W crystals; and during ⟨112⟩ compression, the surface-emanated twin embryos cannot expand

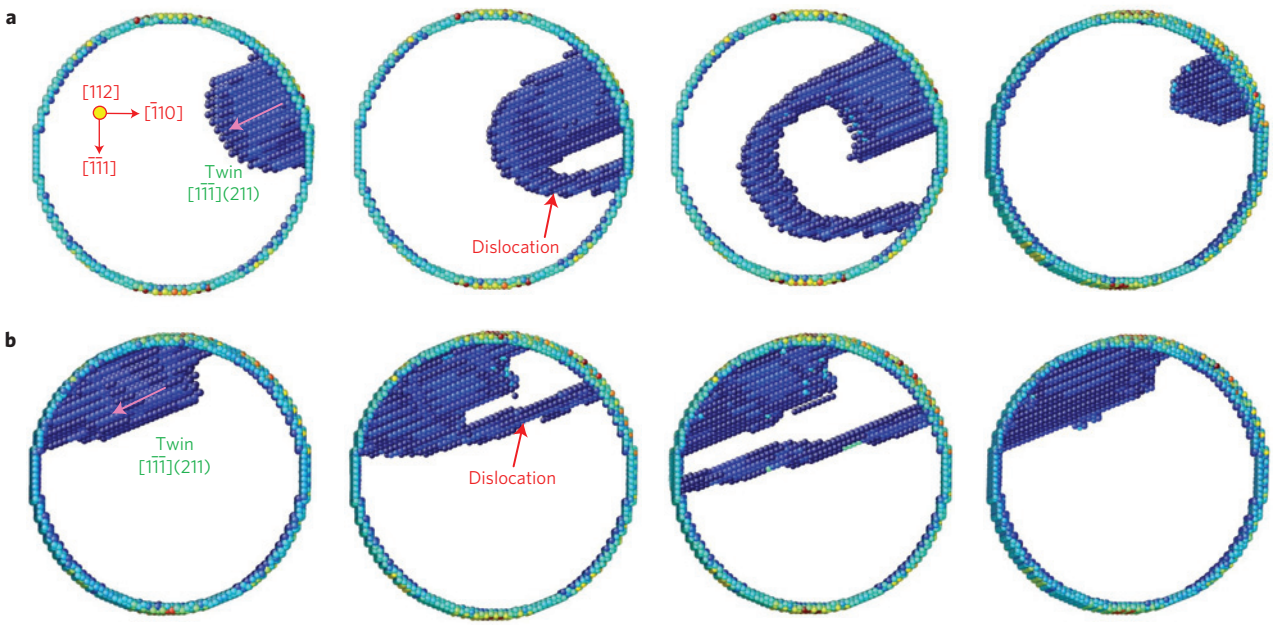

Figure 4 | Atomistic simulations of the competition between twinning and dislocation slip in a W nanowire under [112] compression. a, Sequential snapshots (from the left to right) showing the nucleation and expansion of a dislocation loop from the edge of a pre-embedded twin embryo, whose edge is predominantly perpendicular to the twin shear direction (pink arrow). Atoms are coloured by central symmetry parameters, and those in the perfect lattice are removed for clarity. **b**, Similar to **a**, except that the dominant edge of the twin embryo is parallel to the twin shear direction. In both cases, the expansion of the twin embryo is suppressed due to the competing nucleation of a dislocation that accommodates the load and results in shrinkage of the twin embryo.

due to the competition of dislocation nucleation. These MD results also reinforce the notion of a twinning-dominated deformation mechanism in BCC W nanostructures, except for ⟨112⟩ loading.

Further insights into the competition between deformation twinning and dislocation slip are gained by an analysis of the resolved shear stress on the respective twin and slip systems. At present, there is a lack of established criteria for selecting the active mode of deformation twinning or dislocation slip in BCC metals. However, one expects that the resolved shear stress should play an important role. Table 1 lists the largest Schmid factors of twinning and dislocation slip for each of the four loading orientations tested. Under ⟨110⟩, ⟨100⟩ and ⟨111⟩ axial loadings, the corresponding Schmid factors of twinning are larger by a finite margin than those of dislocation slip. This is consistent with the observed twinning-dominated deformation mechanism in the experiments. However, for ⟨112⟩ axial loading, the Schmid factors of twinning and dislocation slip are very close, which implies similar resolved shear stresses to drive twin formation and dislocation nucleation. In this case, the atomistic simulations shown in Fig. 4 suggest that the dislocation nucleation is favoured, possibly due to the difficulty of lateral expansion of the twin embryo. Nevertheless, a mechanistically based, quantitative criterion for selecting the deformation twinning versus dislocation slip warrants further research in the future.

It is worthwhile comparing and contrasting the deformation mechanisms of FCC and BCC nanostructures. First, mechanical twinning can become the dominant deformation mechanism in both BCC and FCC nanoscale crystals at room temperature and low strain rates. While deformation twinning has been well documented in FCC nanostructures[3,14–16], our work provides the first direct experimental evidence of a twinning-dominated deformation mechanism in BCC W nanostructures. The twinning dominance in nanoscale FCC and BCC metals arises due to prevalent high stresses that favour twinning over dislocation slip. However, unlike FCC metals, twin nucleation in BCC metals is subject to large surface and lattice resistances. Our atomistic simulations suggest that the nucleation of twin embryos can be limited by their lateral expansion under ⟨112⟩ compression, while the vertical twin thickening is relatively easy as it involves the glide of twin interface dislocations with low energy barriers[44]. As a result, dislocation slip can dominate over twinning for certain loading conditions, such as ⟨112⟩ tension and compression in W nanostructures. Second, dislocation starvation is typical in FCC nanostructures[13], but not always observed in the BCC W nanostructures. In BCC nanoscale crystals under ⟨112⟩ loading, numerous nucleation events can occur simultaneously, and a gradual increase in dislocation density occurs during continual straining. This difference may play a role in the observed different strengthening trends in small-scale FCC and BCC single crystals when dislocations dominate the deformation[38,45]. Third, deformation twinning can be pseudoelastic in elemental BCC nanoscale crystals during loading and unloading, as shown in the present work. In contrast, while the deformation-induced twinning has been experimentally observed in FCC nanowires[14–16], the detwinning and pseudoelasticity have not been reported so far. It is also of interest to note that the pseudoelastic deformation has been recently observed in nanoscale shape-memory alloys[46] and ceramics[47]. Pseudoelasticity could allow reversible inelastic deformation, superelasticity, large actuation, energy storage and mechanical damping in micro/nanodevices under high-load conditions[11,46–48]. Finally, we comment that the *in situ* welding technique developed in this work provides a relatively simple and yet effective means of sample preparation to facilitate the *in situ* atomic-scale mechanical testing of nanostructures. Our work also demonstrates the advantage of *in situ* HRTEM deformation experiments that allow the unambiguous determination of active systems of dislocation slip, which has been a challenge for BCC crystals[10,41].

In conclusion, the combined *in situ* TEM experiments and atomistic simulations have revealed that deformation twinning is the dominant deformation mode in BCC W nanoscale crystals at room temperature and low strain rates, when loaded along ⟨100⟩, ⟨110⟩ and ⟨111⟩ directions. Under cyclic loads, deformation twinning is pseudoelastic. Our *in situ* TEM experiments also reveal that

Table 1 | Largest Schmid factors on the dislocation slip and deformation twinning systems for the four loading orientations tested in BCC W nanowires.

Loading orientation	Dislocation		Twinning		Dominant mechanism in experiment
	Slip system	Schmid factor	Twin system	Schmid factor	
[$\bar{1}$10]	1/2[1$\bar{1}$1](1$\bar{0}$1)	0.41	1/6[1$\bar{1}$1](1$\bar{1}$2)	0.47	Twinning
[112]	1/2[1$\bar{1}\bar{1}$](101)	0.41	1/6[1$\bar{1}\bar{1}$](211)	0.39	Dislocation slip
[100]	1/2[11$\bar{1}$](1$\bar{1}$0)	0.41	1/6[11$\bar{1}$](2$\bar{1}$1)	0.47	Twinning
[$\bar{1}$11]	1/2[1$\bar{1}$1](1$\bar{0}$1)	0.27	1/6[1$\bar{1}$1](1$\bar{1}$2)	0.31	Twinning

dislocation plasticity is the primary mode of deformation for ⟨112⟩ loading, resulting in plastic yielding. The loading orientation effect is attributed to the competing nucleation mechanism of defects in small-scale BCC crystals. Broadly, our work demonstrates that the combined *in situ* HRTEM nanomechanical testing and atomistic modelling enable a deeper understanding of the fundamental deformation mechanisms in nanomaterials, and such integrated research may ultimately enable the design of nanostructured materials to realize their latent mechanical strength to the full.

Methods

The *in situ* straining of the nanoscale BCC W crystals (that is, single crystal or bicrystals) was enabled by a unique fabrication method of *in situ* welding inside TEM (see Supplementary Methods for details). In this method, a nanosized sharp tip on the fracture surface of a bulk metallic rod and an electrochemically etched probe were used as the two ends of the nanowire. A voltage, instead of an electrical pulse that tends to produce metallic glasses[49], was pre-applied to one of the two ends. When contact was made, the metallic rod and probe were welded together, forming a crystal nanowire between them. This method allows one to fabricate high-quality nanosized crystal samples *in situ* from bulk metals inside the TEM directly, and subsequent *in situ* nanomechanical testing can be conducted with atomic-scale resolution. This is in contrast to other methods in which pre-synthesized[8,9,17] or pre-fabricated nanosized samples were used[6,7,12,24,28,30]. More importantly, this method can be applied to various types of metals with different crystal structures, such as BCC (Mo, V, Ta) and FCC (Au, Pt) metals. It allows the effective fabrication of clean sub-100 nm metallic samples, in contrast to the commonly used focused ion beam, which causes surface damage and is typically limited to samples greater than 100 nm. Furthermore, this method allows one to control some aspects of the sample geometry (for example, single crystal, bicrystal and nanowires with triple junction), their size (from few nanometres to ~100 nm), orientation, and even surface roughness. Considering the difficulties in handling and testing the nanomaterials, this method provides a relatively simple and yet effective way to study the structure–property relationship in a wide range of small-volume metals and alloys, especially at the atomic scale. Moreover, it may have potential applications in the assembly and interconnection of nanodevices. Further details regarding the experimental and simulation methods can be found in the Supplementary Information.

Received 17 October 2014; accepted 28 January 2015; published online 9 March 2015

References

1. Zhu, T. & Li, J. Ultra-strength materials. *Prog. Mater. Sci.* **55,** 710–757 (2010).
2. Greer, J. R. & DeHosson, J. T. M. Plasticity in small-sized metallic systems: Intrinsic versus extrinsic size effect. *Prog. Mater. Sci.* **56,** 654–724 (2011).
3. Zhu, Y. T., Liao, X. Z. & Wu, X. L. Deformation twinning in nanocrystalline materials. *Prog. Mater. Sci.* **57,** 1–62 (2012).
4. Lu, K., Lu, L. & Suresh, S. Strengthening materials by engineering coherent internal boundaries at the nanoscale. *Science* **324,** 349–352 (2009).
5. Uchic, M. D., Dimiduk, D. M., Florando, J. N. & Nix, W. D. Sample dimensions influence strength and crystal plasticity. *Science* **305,** 986–989 (2004).
6. Shan, Z. W., Mishra, R. K., Syed Asif, S. A., Warren, O. L. & Minor, A. M. Mechanical annealing and source-limited deformation in submicrometre-diameter Ni crystals. *Nature Mater.* **7,** 115–119 (2007).
7. Yu, Q. *et al.* Strong crystal size effect on deformation twinning. *Nature* **463,** 335–338 (2010).
8. Wang, J. W. *et al.* Atomic-scale dynamic process of deformation-induced stacking fault tetrahedra in gold nanocrystals. *Nature Commun.* **4,** 2340 (2013).
9. Wang, J. *et al.* Near-ideal theoretical strength in gold nanowires containing angstrom scale twins. *Nature Commun.* **4,** 1742 (2013).
10. Marichal, C., Van Swygenhoven, H., Van Petegem, S. & Borca, C. {110} Slip with {112} slip traces in bcc tungsten. *Sci. Rep.* **3,** 2547 (2013).
11. Li, L. & Ortiz, C. Pervasive nanoscale deformation twinning as a catalyst for efficient energy dissipation in a bioceramic armour. *Nature Mater.* **13,** 501–507 (2014).
12. Huang, L. *et al.* A new regime for mechanical annealing and strong sample-size strengthening in body centred cubic molybdenum. *Nature Commun.* **2,** 547 (2011).
13. Greer, J. & Nix, W. Nanoscale gold pillars strengthened through dislocation starvation. *Phys. Rev. B* **73,** 245410 (2006).
14. Sedlmayr, A. *et al.* Existence of two twinning-mediated plastic deformation modes in Au nanowhiskers. *Acta Mater.* **60,** 3985–3993 (2012).
15. Yue, Y. *et al.* Quantitative evidence of crossover toward partial dislocation mediated plasticity in copper single crystalline nanowires. *Nano Lett.* **12,** 4045–4049 (2012).
16. Seo, J-H. *et al.* Superplastic deformation of defect-free Au nanowires via coherent twin propagation. *Nano Lett.* **11,** 3499–3502 (2011).
17. Sun, J. *et al.* Liquid-like pseudoelasticity of sub-10-nm crystalline silver particles. *Nature Mater.* **13,** 1007–1012 (2014).
18. Lita, A. E. *et al.* Tuning of tungsten thin film superconducting transition temperature for fabrication of photon number resolving detectors. *IEEE Trans. Appl. Supercond.* **15,** 3528–3531 (2005).
19. Lee, Y-H. *et al.* Tungsten nanowires and their field electron emission properties. *Appl. Phys. Lett.* **81,** 745–747 (2002).
20. Zhang, Y. *et al.* Automated nanomanipulation for nanodevice construction. *Nanotechnology* **23,** 065304 (2012).
21. Swygenhoven, H. V., Derlet, P. M. & Frøseth, A. G. Stacking fault energies and slip in nanocrystalline metals. *Nature Mater.* **3,** 399–403 (2004).
22. Warner, D. H., Curtin, W. A. & Qu, S. Rate dependence of crack-tip processes predicts twinning trends in f.c.c. metals. *Nature Mater.* **6,** 876–881 (2007).
23. Yamakov, V. I. & Glaessgen, E. H. Nanoscale fracture: To twin or not to twin. *Nature Mater.* **6,** 795–796 (2007).
24. Yu, Q. *et al.* The nanostructured origin of deformation twinning. *Nano Lett.* **12,** 887–892 (2012).
25. Christian, J. W. & Mahajan, S. Deformation twinning. *Prog. Mater. Sci.* **39,** 1–157 (1995).
26. Argon, A. S. & Maloof, S. R. Fracture of tungsten single crystals at low temperatures. *Acta Metall.* **14,** 1463–1468 (1966).
27. Chen, C. Q., Florando, J. N., Kumar, M., Ramesh, K. T. & Hemker, K. J. Incipient deformation twinning in dynamically sheared bcc tantalum. *Acta Mater.* **69,** 114–125 (2014).
28. Kim, J-Y., Jang, D. & Greer, J. R. Tensile and compressive behavior of tungsten, molybdenum, tantalum and niobium at the nanoscale. *Acta Mater.* **58,** 2355–2363 (2010).
29. Han, M. S. *et al.* Critical-temperature/Peierls-stress dependent size effects in body centered cubic nanopillars. *Appl. Phys. Lett.* **102,** 041910 (2013).
30. Xie, K. Y. *et al.* The effect of pre-existing defects on the strength and deformation behavior of α-Fe nanopillars. *Acta Mater.* **61,** 439–452 (2013).
31. Marichal, C. *et al.* Origin of anomalous slip in tungsten. *Phys. Rev. Lett.* **113,** 025501 (2014).
32. Chisholm, C. *et al.* Dislocation starvation and exhaustion hardening in Mo alloy nanofibers. *Acta Mater.* **60,** 2258–2264 (2012).
33. Bei, H., Shim, S., Pharr, G. M. & George, E. P. Effects of pre-strain on the compressive stress–strain response of Mo-alloy single-crystal micropillars. *Acta Mater.* **56,** 4762–4770 (2008).
34. Schneider, A. *et al.* Correlation between critical temperature and strength of small-scale bcc pillars. *Phys. Rev. Lett.* **103,** 105501 (2009).
35. Wang, Y. M. *et al.* Deformation twinning during nanoindentation of nanocrystalline Ta. *Appl. Phys. Lett.* **86,** 101915 (2005).
36. Duesbery, M. S. & Vitek, V. Plastic anisotropy in b.c.c. transition metals. *Acta Mater.* **46,** 1481–1492 (1998).
37. Narayanan, S., McDowell, D. L. & Zhu, T. Crystal plasticity model for BCC iron atomistically informed by kinetics of correlated kinkpair nucleation on screw dislocation. *J. Mech. Phys. Solids* **65,** 54–68 (2014).

38. Weinberger, C. R. & Cai, W. Surface-controlled dislocation multiplication in metal micropillars. *Proc. Natl Acad. Sci. USA* **105,** 14304–14307 (2008).
39. Gumbsch, P., Riedle, J., Hartmaier, A. & Fischmeister, H. F. Controlling factors for the brittle-to-ductile transition in tungsten single crystals. *Science* **282,** 1293–1295 (1998).
40. Brunner, D. Comparison of flow-stress measurements on high-purity tungsten single crystals with the kink-pair theory. *Mater. Trans.* **41,** 152–160 (2000).
41. Weinberger, C. R., Boyce, B. L. & Battaile, C. C. Slip planes in bcc transition metals. *Int. Mater. Rev.* **58,** 296–314 (2013).
42. Srivastava, K., Weygand, D. & Gumbsch, P. Dislocation junctions as indicators of elementary slip planes in body-centered cubic metals. *J. Mater. Sci.* **49,** 7333–7337 (2014).
43. Caillard, D. Kinetics of dislocations in pure Fe. Part I. *In situ* straining experiments at room temperature. *Acta Mater.* **58,** 3493–3503 (2010).
44. Ogata, S., Li, J. & Yip, S. Energy landscape of deformation twinning in bcc and fcc metals. *Phys. Rev. B* **71,** 224102 (2005).
45. Greer, J. R., Weinberger, C. R. & Cai, W. Comparing the strength of f.c.c. and b.c.c. sub-micrometer pillars: Compression experiments and dislocation dynamics simulations. *Mater. Sci. Eng. A* **493,** 21–25 (2008).
46. Juan, J. S., Nó, M. L. & Schuh, C. A. Nanoscale shape-memory alloys for ultrahigh mechanical damping. *Nature Nanotechnol.* **4,** 415–419 (2009).
47. Lai, A., Du, Z. H., Gan, C. L. & Schuh, C. A. Shape memory and superelastic ceramics at small scales. *Science* **341,** 1505–1508 (2013).
48. Li, S. *et al.* High-efficiency mechanical energy storage and retrieval using interfaces in nanowires. *Nano Lett.* **10,** 1774–1779 (2010).
49. Zhong, L., Wang, J., Sheng, H., Zhang, Z. & Mao, S. X. Formation of monatomic metallic glasses through ultrafast liquid quenching. *Nature* **512,** 177–180 (2014).

Acknowledgements

S.X.M. acknowledges the support from NSF CMMI 08 010934 through University of Pittsburgh and Sandia National Lab. T.Z. acknowledges the support from DOE NEUP Grant DE-AC07-05ID14517, NSF grant DMR-1410331, and HPC resources in CAS Shenyang Supercomputing Centre. This work was performed, in part, at the Center for Integrated Nanotechnologies, a US Department of Energy, Office of Basic Energy Sciences user facility. This research was supported in part by an appointment to the Sandia National Laboratories Truman Fellowship in National Security Science and Engineering, sponsored by Sandia Corporation (a wholly owned subsidiary of Lockheed Martin Corporation) as Operator of Sandia National Laboratories under its US Department of Energy Contract No. DE-AC04-94AL85000. The authors are grateful to W. Cai of Stanford University, J. Li of Massachusetts Institute of Technology and J. Y. Huang for stimulating discussions.

Author contributions

J.W. designed and conducted experiments, analysed data and wrote the paper under the direction of S.X.M. C.R.W., Z.Zeng and T.Z. performed computer simulations. T.Z., C.R.W. and S.X.M. contributed to data analysis and revised the paper. All the authors contributed to the discussion.

Additional information

Supplementary information is available in the online version of the paper. Reprints and permissions information is available online at www.nature.com/reprints.
Correspondence and requests for materials should be addressed to C.R.W., T.Z. or S.X.M.

Competing financial interests

The authors declare no competing financial interests.